

Commun. Theor. Phys. **74** (2022) 075702 (8pp) https://doi.org/10.1088/1572-9494/ac75db

Topological and dynamical phase transitions in the Su–Schrieffer–Heeger model with quasiperiodic and long-range hoppings

Wei-Jie Zhang[1], Yi-Piao Wu[1], Ling-Zhi Tang[1] and Guo-Qing Zhang[1,2]

[1] Guangdong Provincial Key Laboratory of Quantum Engineering and Quantum Materials, School of Physics and Telecommunication Engineering, South China Normal University, Guangzhou 510006, China
[2] Guangdong-Hong Kong Joint Laboratory of Quantum Matter, Frontier Research Institute for Physics, South China Normal University, Guangzhou 510006, China

E-mail: zhangptnoone@m.scnu.edu.cn

Received 2 March 2022, revised 6 June 2022
Accepted for publication 6 June 2022
Published 1 July 2022

Abstract

Disorders and long-range hoppings can induce exotic phenomena in condensed matter and artificial systems. We study the topological and dynamical properties of the quasiperiodic Su–Schrier–Heeger model with long-range hoppings. It is found that the interplay of quasiperiodic disorder and long-range hopping can induce topological Anderson insulator phases with non-zero winding numbers $\omega = 1, 2$, and the phase boundaries can be consistently revealed by the divergence of zero-energy mode localization length. We also investigate the nonequilibrium dynamics by ramping the long-range hopping along two different paths. The critical exponents extracted from the dynamical behavior agree with the Kibble–Zurek mechanic prediction for the path with $W = 0.90$. In particular, the dynamical exponent of the path crossing the multicritical point is numerical obtained as $1/6 \sim 0.167$, which agrees with the unconventional finding in the previously studied XY spin model. Besides, we discuss the anomalous and non-universal scaling of the defect density dynamics of topological edge states in this disordered system under open boundary condictions.

Keywords: topological Anderson insulator, higher winding number, Kibble–Zurek machanic

(Some figures may appear in colour only in the online journal)

1. Introduction

Topological insulators, characterized by topological invariants and non-trivial surface states, have witnessed fast development in condensed-matter [1, 2] and tunable artificial systems [3–14]. In general, topological insulators are robust against certain types of weak disorder due to symmetric protection. However, in the presence of strong disorder, the system usually becomes trivial insulators due to the Anderson localization [15]. The nontrivial interplay between topology and localization leads to a surprising phenomenon of topological Anderson insulators (TAIs), which is an exotic topological phase induced by moderate disorders [16]. The disorder-induced topological phase transitions and TAIs have been widely studied [16–41] and experimental evidenced in various systems [37, 42–46] such as ultracold atom [44] and photonic waveguide array [46]. Notably, random disorders attached to on-site potentials or hopping terms are mainly considered in most of these works. It has been shown that quasiperiodic disorder can lead to unique localization behaviors, such as localization transition [47, 48] and intermediate or critical phases [49–55]. In addition, the presence of long-range hopping in disordered systems can give rise to the power-law localization [56–59], and the topological phases are studied in extended Su–Schrieffer–Heeger (SSH) model with long-range hoppings [60–63]. However, the topological phase transition due to the interplay of quasiperiodic disorder and long-range hopping remains largely unexplored.

On the other hand, non-equilibrium dynamics hold a complementary and important way to explore the phase

transitions. In particular, the Kibble–Zurek mechanics (KZM) [64, 65] have been proposed to study the universal dynamical properties of second-order phase transitions with parameter ramping. According to KZM [64–67], the non-equilibrium dynamics react to the phase transition near the critical point and is immune to the detail setting. The excitation production obeys the power-law scaling with respect to the quench velocity. This can be vividly understood that the slower system moves, the less excitation comes into forge due to the loss of adiabaticity when crossing the critical point. The power-law exponent can be determined by the universal exponents, such as correlation length exponent and dynamical exponent. In experiments, the KZM of dynamical phase transitions has been observed in superfluid [68], Bose–Einstein condensation [69–71], trapped ions [72–75], and superconducting circuits [76, 77]. Recently, considerable effort is devoted to studying the dynamical phase transitions in topological systems [78–87]. For the dynamical topological phase transition, the edge states may exhibit anomalous scaling [78–80] and the local Berry curvature [86] and topological marker [86] can be connected to the characteristic correlation length in the context of the KZM. In addition, the characteristic correlation length is also verified in the localization transition in the presence of disorders [88, 89]. However, the dynamical phase transition with the KZM in disordered topological systems is still less understood [86].

In this work, we study the topology, localization, and dynamics of the quasiperiodic SSH model with next-next-nearest-neighbor (NNNN) long-range hoppings. Firstly, we numerically compute the topological phase diagram by the real-space winding number to characterize the effects of disorder and long-range hopping. We find a higher winding number TAI phase together with other two different phases which consist a multicritical point. The topological phase boundaries are also characterized by the divergence of the zero-energy mode localization length. We then investigate the localization property by using the inverse partition ratio of eigenstates. The disorder induced extend to localization transition and non-trivial to trivial transition as well as a fully localized TAI region are observed. Furthermore, we extend our study to the nonequilibrium dynamics and study the KZM with topological phase transitions by ramping the long-range hopping strength along two representative paths in the topological phase diagram. The critical exponents numerical calculated from the dynamical behavior is consistent with the KZM power-law scaling prediction for one path with $W = 0.90$, and the dynamical exponent for the path crossing the multicritical point is the same as the previously studied XY model. In addition, we discuss the defect density dynamics of the topological edge states and show their anomalous and non-universal scaling in this disordered system.

The rest of this paper is organized as follows. The extended SSH model with quasiperiodic disordered and long-range hoppings is proposed in section 2. Section 3 is devoted to studying the topological phase transitions and TAIs. In section 4, we explore the dynamical phase transition with the KZM in this disordered topological system. A brief conclusion is given in section 5.

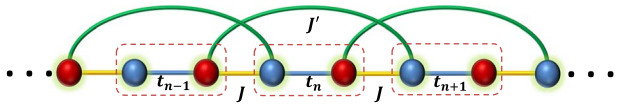

Figure 1. The sketch of the extended SSH model with the incommensurate intracell hopping (t_n), the intercell hopping (J) and the long-range NNNN hopping (J'). Blue and red balls indicate sublattices A and B in a unit cell circled by the dashed square.

2. Model

We consider the extended SSH model consisting of two sublattices A and B in a unit cell with an additional NNNN hopping, as shown in figure 1. The corresponding tight-binding Hamiltonian reads

$$H = J\sum_n (c^\dagger_{A,n+1}c_{B,n} + \text{h.c.}) + \sum_n (t_n c^\dagger_{A,n}c_{B,n} + \text{h.c.}) + J'\sum_n (c^\dagger_{A,n+2}c_{B,n} + \text{h.c.}), \quad (1)$$

where $c^\dagger_{A(B),n}$ and $c_{A(B),n}$ denote the creation and annihilation operators on sublattice A(B) in the nth unit cell, J is the nearest-neighbor intercell hopping, and J' is the NNNN hopping between different sublattices. We further consider the quasiperiodic disordered intracell hopping t_n with the incommensurate modulation form [90, 91]

$$t_n = m + W\cos(2\pi\alpha n + \phi), \quad (2)$$

where α is an irrational number, ϕ is a random phase for sampling, m is the overall hopping strength, and W is the quasiperiodic disorder strength. We consider the model of N unit cells with a total number of $2N$ sublattice sites. This model with the disordered and long-range hoppings still satisfies the chiral symmetry [92] $\Gamma^{-1}H\Gamma = -H$ as only hoppings between different sublattices are contained, where $\Gamma = I_N \otimes \sigma_z$ being the chiral operator, I_N is the identity operator, and σ_z the Pauli matrix. For simplicity and without the loss of generality, we set $J = 1$ as the energy unit and $\alpha = (\sqrt{5} - 1)/2$ as the golden ratio.

In the clean limit, the topology of the SSH model can be characterized by the winding number of Bloch vectors in the momentum space. However, the translational symmetry is broken in the presence of disorders. We can use the real-space winding number in a spectral projection method [21, 93] to characterize the bulk topology. The real-space winding number is given by [21, 93]

$$\omega = \frac{1}{N'}\text{Tr}'(\Gamma Q[Q, X]), \quad (3)$$

where $X = \text{diag}(1, 1, 2, 2, \cdots, N, N)$ denotes the position operator and $Q = \sum_{\beta=1}^{2N}|\beta\rangle\langle\beta| - \Gamma^{-1}|\beta\rangle\langle\beta|\Gamma$ is the homotopically equivalent flat-band Hamiltonian matrix, $|\beta\rangle$ is the eigenstate of eigenenergy E_β. In order to avoid the boundary effect, we trace over the middle part with $N' = N/2$ unit cells denoting as Tr′ in equation (3).

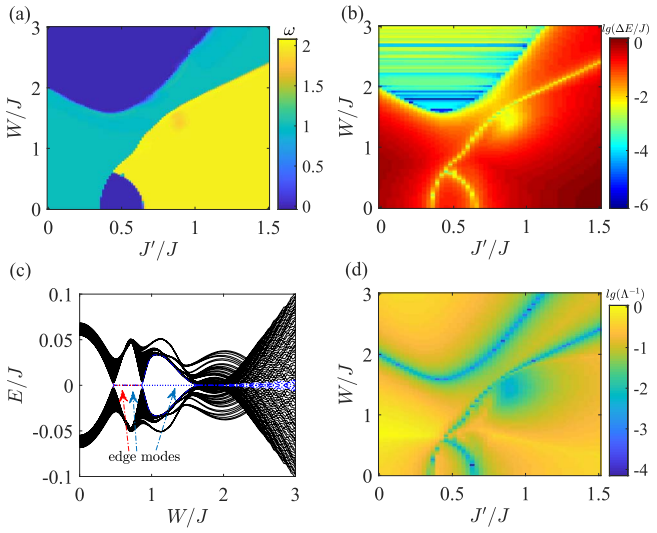

Figure 2. (a) Topological phase diagram in the J'–W plane. (b) Logarithm plot of the bulk energy band gap ΔE under PBCs. (c) Eigenenergies at the middle of the energy spectrum plotted as a function of W for $J' = 0.55$ under OBCs, where the red arrow indicates the second centered pair of edge modes (red dotted lines) and the blue arrows mark the most centered pair of edge modes (blue solid lines). (d) Logarithm plot of the inverse localization length Λ^{-1} computed by the transfer matrix method. Other parameters are $N = 987$, $m = 0.65$, $\phi = 0$.

3. Topological phase transitions

We now study the topological properties of the system in the static case. In figure 2(a), we present the topological phase diagram revealed by the real-space winding number in the W-J' plane for $\phi = 0$ and $m = 0.65$. As shown in figure 2(a), when $W = 0$, the topological phase transition for $\omega = 1 \to \omega = 0$ happens at $J' = J - m = 0.35$, and the topological phase transition for $\omega = 0 \to \omega = 2$ occurs at $J' = m = 0.65$. Thus, the long-range NNNN hopping can induce the topological phase with a high winding number ($\omega = 2$) and related topological transitions even in the clean limit [60, 63, 94]. When the quasiperiodic disorder is considered, there are more topological phase transitions induced by the interplay between the disorder strength W and long-range hopping strength J'. For instance, the topological phase transitions $\omega = 1 \to \omega = 2, \omega = 1 \to \omega = 0 \to \omega = 2$, and $\omega = 1 \to \omega = 0 \to \omega = 1 \to \omega = 2$ can be induced by increasing J' for different fixed values of W. In addition, the topological phase transitions $\omega = 0 \to \omega = 1 \to \omega = 0$ and $\omega = 0 \to \omega = 2 \to \omega = 1 \to \omega = 0$ can be induced by increasing W for $0.35 \lesssim J' \lesssim 0.65$. This indicates the disorder-induced TAI from the trivial phase, which becomes trivial insulators under strong disorder. We can also find that the long-range NNNN hopping significantly enlarges the topological region when $J' > m$.

To reveal the behavior of the bulk gap with respect to the topological phase transitions, we calculate the gap ΔE given by the difference of the most centered two eigenenergies:

$$\Delta E = E_{N+1} - E_N, \tag{4}$$

under the PBC. In figure 2(b), we plot ΔE in the log scale. The bulk gap closes and reopens when crossing the topological phase boundaries, which are consistent with the topological phase diagram shown in figure 2(a). Note that the bulk gaps in two trivial regions are significantly different. For large W, the bulk gap tends to close and the system is a trivial gapless Anderson insulator, while the bulk gap is not closed and the system is a band insulator for small W and moderate J'. We further show the bulk-boundary correspondence which relates the winding number with the edge states under OBC. In figure 2(c), we plot the most centered energy spectrum as a function of W under OBC with fixed $J' = 0.55$. There is an energy gap for $W \lesssim 0.48$, where the system is in the band insulator region. When $0.48 \lesssim W \lesssim 0.86$, two pairs of zero-energy edge modes (blue solid lines and red dot lines) exhibit, corresponding to the TAI phase with $\omega = 2$. When $0.86 \lesssim W \lesssim 1.64$, one of the two pairs of edge modes disappears and the system becomes another TAI phase with $\omega = 1$. When $W \gtrsim 1.64$, the upper and lower bands are mixed due to strong disorder and the system is in the trivial gapless phase.

The zero-energy eigenstates related to the topological phase transitions are exponentially localized and their localization length Λ will be divergent at the transition points [21, 63]. To further reveal the topological transitions, we numerically calculate the localization length by using the transfer matrix method [95]. Expanding the Schrödinger equation $H \mid \varphi\rangle = E \mid \varphi\rangle$ in matrix element in the basis of $\varphi = [\varphi_{1,A}, \varphi_{1,B} \cdots \varphi_{N,A}, \varphi_{N,B}]^{\mathrm{T}}$, we can readily obtain the following iteration relation

$$\begin{pmatrix} \varphi_{n,A} \\ \varphi_{n,B} \\ \varphi_{n+1,A} \\ \varphi_{n+1,B} \end{pmatrix} = T_n \begin{pmatrix} \varphi_{n-1,A} \\ \varphi_{n-1,B} \\ \varphi_{n,A} \\ \varphi_{n,B} \end{pmatrix}, \tag{5}$$

where the transfer matrix for the n-unit cell is written as [63]

$$T_n = \begin{pmatrix} 0 & 0 & 1 & 0 \\ 0 & 0 & 0 & 1 \\ -\frac{t_{n-1}}{J_2} & \frac{E}{J_2} & -\frac{1}{J_2} & 0 \\ -\frac{Et_{n-1}}{J_2 t_{n+1}} & \frac{E^2 - J_2^2}{J_2 t_{n+1}} & -\frac{E}{J_2 t_{n+1}} & -\frac{1}{t_{n+1}}, \end{pmatrix}, \tag{6}$$

which takes $J = 1$ and depends on the quasiperiodic disorder strength t_n (see equation (2)). The localization length Λ of zero-energy eigenstate with $E = 0$ can be iteratively calculated based on the following matrix

$$\Upsilon = \lim_{N \to \infty} \frac{\ln|T_1^\dagger T_2^\dagger \cdots T_N^\dagger T_N \cdots T_2 T_1|}{2N}, \tag{7}$$

with the smallest positive eigenvalue being denoted by $\gamma_{\min}$. The inverse of the localization length of the zero-energy mode Λ^{-1} is then obtained as

$$\Lambda^{-1} = \gamma_{\min}. \tag{8}$$

In figure 2(d), we show the numerical results of Λ^{-1} in the log scale. One can find the vanishing of Λ^{-1} for the divergence of localization length ($\Lambda \to \infty$) accurately characterizes the boundaries of different topological phases. The results not only show the trivial-nontrivial phase transitions but also

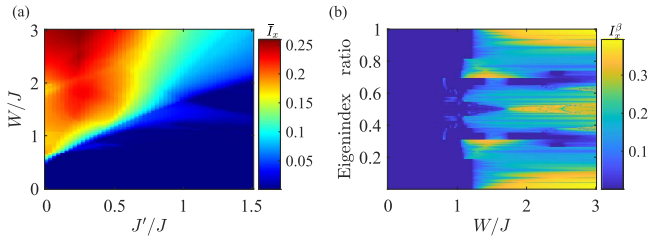

Figure 3. (a) Real-space eigenstate-averaged IPR $\bar{I}_x$, and (b) real-space IPR of each eigenstate I_x^β as a function of W for $J' = 0.55$ under the PBC. Other parameters are $N = 987$, $m = 0.65$, $\phi = 0$.

reveal that transition between two different topological phases with $\omega = 1$ and $\omega = 2$ in this disordered long-ranged SSH model.

To study the localization effect of the quasiperiodic disorder on the bulk state, we numerically compute the inverse partition ratio (IPR) for each eigenstate I_x^β in real space as

$$I_x^\beta = \sum_{n=1}^{2N} |\langle n \mid \beta\rangle|^4, \tag{9}$$

where $\{|\, n\rangle\}$ is the complete set of the real space basis and $|\, \beta\rangle$ is the β-th eigenstate. An eigenstate is extended when $I_x^\beta \sim 1/N$. The overall localization of the bulk states can be characterized by the eigenstate-averaged IPR:

$$\bar{I}_x = \frac{1}{2N}\sum_{\beta=1}^{2N} I_x^\beta. \tag{10}$$

In figure 3(a), we show $\bar{I}_x$ as functions of W and J'. One can see that the disorder W drives the bulk states more localized while the NNNN hopping J' tends to make them delocalized. This can be intuitively understood that the long-range hopping serves as another channel for a particle to move between sites and thus enhances the possibility of particle delocalization. In figure 3(b), we plot the real-space IPR of each eigenstate I_x^β as a function of W for $J' = 0.55$. For small W, the bulk states are fully extended with a vanishing $\bar{I}_x$. There is a transition from the extended phase to localized phase at $W \approx 1.06$ before the system turns into a trivial Anderson insulator at $W \approx 1.64$.

4. Dynamical phase transitions

In this section, we study the nonequilibrium dynamical phase transitions in this model based on the KZM with the critical exponents. It has been known that the KZM predicts the defect density based on the analysis of critical slowing down phenomenon and the static critical exponents [66, 96–98]. Here we focus on the quantum quench [88, 89, 99] of the long-range hopping J' for two fixed typical disorder strengths. The first quench is from the topological phase with $\omega = 1$ to the one with $\omega = 2$ for $W = 0.90$. Another quench path crosses the multicritical point at $W = 0.61$. To this end, we first calculate the correlation length exponent ν via

$$\Lambda \sim \varepsilon^{-\nu} = |J' - J_c'|^{-\nu}, \tag{11}$$

where the localization length Λ (see equation (8)) is taken as

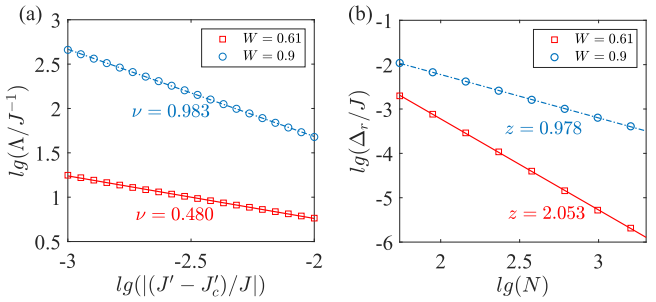

Figure 4. (a) Scaling relations between localization length Λ and critical distance $\varepsilon = |\, J' - J_c'\,|$ for two quench paths with the system size $N = 987$. For $W = 0.90$, $J_c' \approx 0.5632$, while for $W = 0.61$, $J_c' \approx 0.4391$. (b) Scaling relations between relevant gap Δ_r and the system size N near the critical point J_c'. Correlation length exponents ν and dynamical exponents z are labeled to the corresponding linearly fitting lines. All data points are obtained under OBCs and averaged over 100 random configurations of phases ϕ. Other parameter is $m = 0.65$.

the correlation length for the topological phases here, J_c' is the critical point of the respective phase transition, and ε the distance from current quenching J' to the critical point J_c'. By numerically computing Λ from the transfer matrix method, we can determine the correlation length exponent ν. We plot the numerical data as well as a log–log linear fit to those data in figure 4(a), and all points are disorder averaged from 100 random configurations by ϕ s. For the first quench path with $W = 0.90$ and $J_c' \approx 0.5632$, we obtain the correlation length exponent $\nu \approx 0.983 \pm 0.005$. For the second quench path crossing the multicritical point at $W = 0.61$ with $J_c' \approx 0.4391$, we obtain $\nu \approx 0.480 \pm 0.005$.

The dynamical exponent z can be extracted from the finite-size scaling of the relevant gap Δ_r as

$$\Delta_r \sim N^{-z}, \tag{12}$$

near the critical point J_c'. We define the second positive energy E_{N+2} under OBCs as the relevant gap Δ_r, which is in accordance with the defect density defined and investigated later in this section. Figure 4(a) displays the numerical results of the dynamic exponents z obtained from the finite-size scaling of the relevant gap Δ_r. We obtain $z \approx 0.978 \pm 0.012$ and $z \approx 2.053 \pm 0.021$ for the first and second quenches of J' with fixed $W = 0.90$ and $W = 0.61$, respectively.

We proceed to relate the obtained correlation-length and dynamical exponents to the scaling of the defect density after the quench dynamics, as predicted by the KZM. At the initial time t_0, the system is prepared far away from the topological phase transition point, and the initial state which occupies half the lowest single-particle energy levels (up to a normalization constant) reads

$$|\psi(t_0)\rangle = \frac{1}{\sqrt{N}}\sum_{\beta=1}^{N} |\beta_{\text{instan}}(t_0)\rangle, \tag{13}$$

where $|\beta_{\text{instan}}(t_0)\rangle$ is the instantaneous eigenstate of the Hamiltonian at t_0. We consider the quench parameter in a

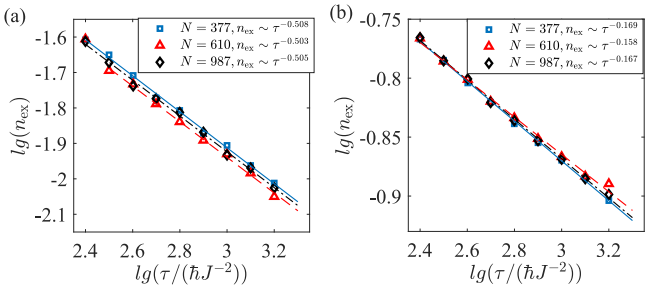

Figure 5. Kibble–Zurek scaling between the defect density n_{ex} and the quench time τ for quenching the long-range hopping stength J' for $W = 0.9$ (a) and $W = 0.61$ (b), respectively. Here n_{ex} is averaged over 80 random configurations of phases ϕ for system sizes $N = 377, 610, 987$ under the PBC. The other parameter is $m = 0.65$.

linear form

$$J'(t) = J'_0 + \frac{t}{\tau}, \tag{14}$$

where J'_0 is the initial hopping parameter at the beginning t_0 and τ is the quench time controlling the evolution velocity. As the system time t evolves and crosses the topological phase transition point, the time-evolution state $|\psi(t)\rangle$ undergoes an adiabatic–diabatic–adiabatic process, which can be numerically obtain by solving the time-dependent Schrödinger equation. The state can be excited to the upper band in the diabatic regime and then the defect density n_{ex} products after the quench. As a consequence of disorder effects, the dynamic behavior can no longer be separated into independent series of subspaces like the Landau–Zener tunneling [100, 101]. When the population transition happens, the evolved state interferes with all energy levels and one can define the defect density as [78]

$$n_{ex} = \sum_{E_\beta > 0} |\langle \beta_{instan}(t_f) | \psi(t_f)\rangle|^2, \tag{15}$$

where the defect density is counted by the probability occupying the upper half bands at the final time t_f, i.e. the states with energies E_β higher than the Fermi energy $E_F = 0$.

Based on the KZM argument for the dynamical phase transitions, the system gets frozen within the magnitude of the frozen time $\hat{t}$ in the vicinity of the critical region (near J'_c in our cases). The frozen time $\hat{t}$ can be determined by the diabatic condition when the relevant gap Δ_r equals to the transition rate $\partial_t \varepsilon/\varepsilon$. According to the argument of the critical slowing down theory, the relevant gap near the critical point is $\Delta_r \sim \varepsilon^{z\nu}$ with $\varepsilon \equiv |\hat{t}/\tau|$, and the transition rate is given as $\partial_t \varepsilon/\varepsilon = |1/\hat{t}|$. We can obtain $\hat{t} \sim \tau^{z\nu/(1+z\nu)}$ when $\Delta_r = \partial_t \varepsilon/\varepsilon$ [96]. Since the defect density can be given by $n_{ex} \sim \Lambda^{-d}$ and the localization length $\Lambda \sim \varepsilon^{-\nu} = |\hat{t}/\tau|^{-\nu}$, one finally obtain

$$n_{ex} \sim \tau^{-\alpha}, \alpha = \frac{dv}{1 + zv}, \tag{16}$$

as the Kibble–Zurek scaling law of the defect production after the dynamical phase transition.

In figure 5, we show our numerical results of the defect density n_{ex} as functions of τ in log–log scale, obtained from real-time dynamics for three system sizes $N = 377, 610, 987$. Data points are averaged over 80 random configurations and the linear fittings are conducted to extract the power-law exponents of the Kibble–Zurek scalings, which converge for the three system sizes investigated. As shown in figure 5(a) for the dynamical topological phase transition for $W = 0.9$, the power-law exponents extracted from dynamics are respectively $\alpha \approx 0.508, 0.503, 0.505$ for $N = 377, 610, 987$, which are consisting with the theoretical prediction of KZM $n_{ex} \sim \tau^{-0.501}$, via combining critical exponents z and ν in equation (16) with $d = 1$. However, figure 5(b) shows the obtained power-law exponents $\alpha \approx 0.169, 0.158, 0.167$ for $N = 377, 610, 987$, respectively. The exponents violate the conventional KZM prediction with $n_{ex} \sim \tau^{-0.242}$ as the evolution path crosses the multicritical point in this case. However, quenching through the multicritical point in the XY spin model takes the modified Kibble–Zurek scaling of the defect density $n_{ex} \sim \tau^{-1/6}$ as their critical exponents should be $\nu = 0.5$ and $z = 2$, which belongs to Lifshitz universal class [102]. Thus, our numerical results of $\nu \approx 0.480 \pm 0.005$, $z \approx 2.053 \pm 0.021$ and $\alpha \approx 0.169, 0.158, 0.167$ agree with the theoretical predictions for multicritical point cases with $\alpha = 1/6 \sim 0.167$ [102]. Note that the calculation of the effective critical exponents for the multicritical point in the XY model [102] cannot be directly used in our model since the quasiperiodic disorder breaks the translation invariance. A natural conjecture is to adapt the recently proposed self-consistent Born approximation method [17, 29] to smooth disorders into an effective momentum space Hamiltonian, and then figure out the effective critical exponents. We leave the deduction of the effective critical exponents at the multicritical point in disordered systems for further studies.

As revealed in [78, 80], the topological edge states can cause the anomalous and non-universal scaling of defect dynamics in clean systems under the open boundary condiction. To reveal this scaling behavior in our disordered system, we simulate the dynamics of the topological edge states under the parameter quench from $\omega = 1$ to $\omega = 2$ in the topological phase diagram under the open boundary condiction. As shown in figure 6, we plot typical results of the scaling between the defect density n_{ex} and the quench time τ. We can find the topological edge states result in the anomalous scaling, which cannot be predicted by the static critical exponents based on the Kibble–Zurek mechanism. The scaling exponents are bigger than the Kibble–Zurek exponents resulting from bulk states, indicating that topological edge states may be more stable in the quench process. The scaling of topological edge states dynamics is also not universal and depends on the disorder strength.

5. Conclusion

In summary, we have investigated topological phases, localization transition, and KZM critical exponents of the extended SSH model with quasiperiodic disordered and long-range

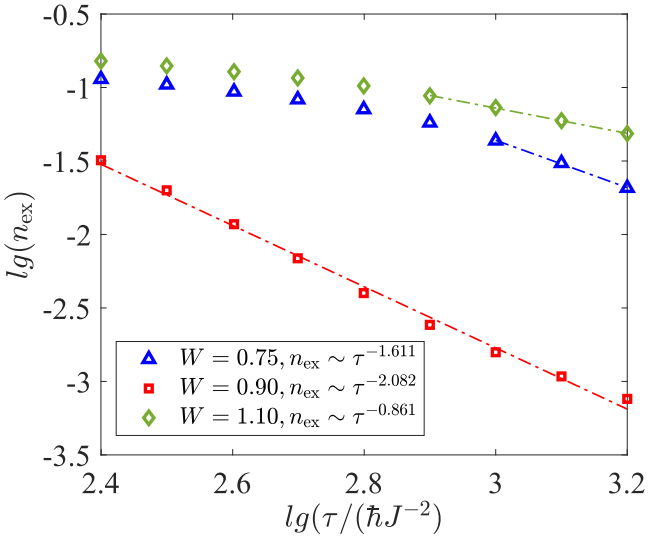

Figure 6. Scaling between the defect density n_{ex} and the quench time τ for quenching the long-range hopping stength J' for $W = 0.75, 0.90, 1.10$ under the open boundary condiction. The initial state is prepared as the equal weight of two topological edge states in the region of $\omega = 1$. n_{ex} is averaged over 80 random configurations of phases ϕ for system sizes $N = 987$. The other parameter is $m = 0.65$.

hopping. The phase diagram revealed by the real-space winding number shows a higher winding number $\omega = 2$ region, and boundaries of different topological phases characterized by bulk gap closing under PBCs are consistent with those indicated by the winding number. Moreover, the zero-energy modes under OBCs indicate the number of pairs of edge modes in the TAI region. The divergence of zero modes localization length can also mark the topological phase transition and reveal the $\mathbb{Z}$ classification of the topological index. We have calculated the eigenstate-averaged real-space IPR and IPR of each eigenstate to reveal the localization properties. Disorder W can drive the system from extend to localized and from topological non-trivial to trivial regions, and a fully localized TAI occurs before the system is driven into a trivial Anderson insulator. We have also investigated the nonequilibrium dynamical behavior in terms of the KZM with a topological phase transition or crossing the multicritical point. We have calculated the critical exponents ν and z by numerical scalings of physical quantities. The dynamically extracted exponent is consistent with the theoretical prediction of KZM for $W = 0.90$, while dynamical and static exponents of the other ramping path crossing the multicritical point agree with the previously studied XY model. Finally, we have shown that the topological edge states result in anomalous scaling, which is non-universal and depends on the disorder strength.

Acknowledgments

The authors thank D-W Zhang for helpful discussions. This work was supported by the National Natural Science Foundation of China (Grant No. 12104166), the Key-Area Research and Development Program of Guangdong Province (Grant No. 2019B030330001), the Science and Technology of Guangzhou (Grant No. 2019050001), and the Guangdong Basic and Applied Basic Research Foundation (Grant No. 2020A1515110290).

ORCID iDs

Guo-Qing Zhang https://orcid.org/0000-0001-6124-4998

References

[1] Qi X-L and Zhang S-C 2011 Topological insulators and superconductors *Rev. Mod. Phys.* **83** 1057
[2] Hasan M Z and Kane C L 2010 Colloquium: topological insulators *Rev. Mod. Phys.* **82** 3045
[3] Zhang D-W, Zhu Y-Q, Zhao Y X, Yan H and Zhu S-L 2018 Topological quantum matter with cold atoms *Adv. Phys.* **67** 253
[4] Cooper N R, Dalibard J and Spielman I B 2019 Topological bands for ultracold atoms *Rev. Mod. Phys.* **91** 015005
[5] Goldman N, Budich J C and Zoller P 2016 Topological quantum matter with ultracold gases in optical lattices *Nat. Phys.* **12** 639
[6] Schroer M D, Kolodrubetz M H, Kindel W F, Sandberg M, Gao J, Vissers M R, Pappas D P, Polkovnikov A and Lehnert K W 2014 Measuring a topological transition in an artificial spin-1/2 system *Phys. Rev. Lett.* **113** 050402
[7] Roushan P *et al* 2014 Observation of topological transitions in interacting quantum circuits *Nature* **515** 241
[8] Tan X, Zhang D-W, Liu Q, Xue G, Yu H-F, Zhu Y-Q, Yan H, Zhu S-L and Yu Y 2018 Topological Maxwell metal bands in a superconducting qutrit *Phys. Rev. Lett.* **120** 130503
[9] Tan X *et al* 2019 Experimental measurement of the quantum metric tensor and related topological phase transition with a superconducting qubit *Phys. Rev. Lett.* **122** 210401
[10] Lee C H, Imhof S, Berger C, Bayer F, Brehm J, Molenkamp L W, Kiessling T and Thomale R 2018 Topolectrical circuits, communications *Physics* **1** 39
[11] Huber S D 2016 Topological mechanics *Nat. Phys.* **12** 621
[12] Lu L, Joannopoulos J D and Soljačić M 2014 Topological photonics *Nat. Photonics* **8** 821
[13] Ozawa T *et al* 2019 Topological photonics *Rev. Mod. Phys.* **91** 015006
[14] Zhang D-W, Zhao Y X, Liu R-B, Xue Z-Y, Zhu S-L and Wang Z D 2016 Quantum simulation of exotic PT-invariant topological nodal loop bands with ultracold atoms in an optical lattice *Phys. Rev.* A **93** 043617
[15] Anderson P W 1958 Absence of diffusion in certain random lattices *Phys. Rev.* **109** 1492
[16] Li J, Chu R-L, Jain J K and Shen S-Q 2009 Topological Anderson insulator *Phys. Rev. Lett.* **102** 136806
[17] Groth C W, Wimmer M, Akhmerov A R, Tworzydło J and Beenakker C W J 2009 Theory of the topological Anderson insulator *Phys. Rev. Lett.* **103** 196805
[18] Jiang H, Wang L, Sun Q-F and Xie X C 2009 Numerical study of the topological Anderson insulator in HgTe/CdTe quantum wells *Phys. Rev.* B **80** 165316
[19] Guo H-M, Rosenberg G, Refael G and Franz M 2010 Topological Anderson insulator in three dimensions *Phys. Rev. Lett.* **105** 216601
[20] Altland A, Bagrets D, Fritz L, Kamenev A and Schmiedt H 2014 Quantum criticality of quasi-one-dimensional topological Anderson insulators *Phys. Rev. Lett.* **112** 206602

[21] Mondragon-Shem I, Hughes T L, Song J and Prodan E 2014 Topological criticality in the chiral-symmetric AIII class at strong disorder *Phys. Rev. Lett.* **113** 046802

[22] Titum P, Lindner N H, Rechtsman M C and Refael G 2015 Disorder-induced Floquet topological insulators *Phys. Rev. Lett.* **114** 056801

[23] Wu B, Song J, Zhou J and Jiang H 2016 Disorder effects in topological states: brief review of the recent developments *Chin. Phys.* B **25** 117311

[24] Sriluckshmy P V, Saha K and Moessner R 2018 Interplay between topology and disorder in a two-dimensional semi-Dirac material *Phys. Rev.* B **97** 024204

[25] Zheng J-H, Qin T and Hofstetter W 2019 Interaction-enhanced integer quantum Hall effect in disordered systems *Phys. Rev.* B **99** 125138

[26] Kuno Y 2019 Disorder-induced Chern insulator in the Harper–Hofstadter–Hatsugai model *Phys. Rev.* B **100** 054108

[27] Chen R, Xu D-H and Zhou B 2019 Topological Anderson insulator phase in a quasicrystal lattice *Phys. Rev.* B **100** 115311

[28] Wang X S, Brataas A and Troncoso R E 2020 Bosonic Bott index and disorder-induced topological transitions of magnons *Phys. Rev. Lett.* **125** 217202

[29] Li C-A, Fu B, Hu Z-A, Li J and Shen S-Q 2020 Topological phase transitions in disordered electric quadrupole insulators *Phys. Rev. Lett.* **125** 166801

[30] Yang Y-B, Li K, Duan L-M and Xu Y 2021 Higher-order topological Anderson insulators *Phys. Rev.* B **103** 085408

[31] Velury S, Bradlyn B and Hughes T L 2021 Topological crystalline phases in a disordered inversion-symmetric chain *Phys. Rev.* B **103** 024205

[32] Zhang D-W, Tang L-Z, Lang L-J, Yan H and Zhu S-L 2020 Non-Hermitian topological Anderson insulators *Sci. China Phys. Mech. Astron.* **63** 267062

[33] Luo X.-W. and Zhang C. 2019 Non-Hermitian disorder-induced topological insulators arXiv:1912.10652v1 [cond-mat.mes-hall]

[34] Wu H and An J-H 2020 Floquet topological phases of non-Hermitian systems *Phys. Rev.* B **102** 041119

[35] Tang L-Z, Zhang L-F, Zhang G-Q and Zhang D-W 2020 Topological Anderson insulators in two-dimensional non-Hermitian disordered systems *Phys. Rev.* A **101** 063612

[36] Liu H, Su Z, Zhang Z-Q and Jiang H 2020 Topological Anderson insulator in two-dimensional non-Hermitian systems *Chin. Phys.* B **29** 050502

[37] Lin Q, Li T, Xiao L, Wang K, Yi W and Xue P 2021 Observation of non-Hermitian topological Anderson insulator in quantum dynamics arXiv:2108.01097 [cond-mat.mes-hall]

[38] Claes J and Hughes T L 2021 Skin effect and winding number in disordered non-Hermitian systems *Phys. Rev.* B **103** L140201

[39] Zhang G-Q, Tang L-Z, Zhang L-F, Zhang D-W and Zhu S-L 2021 Connecting topological Anderson and Mott insulators in disordered interacting Fermionic systems *Phys. Rev.* B **104** L161118

[40] Li K, Wang J-H, Yang Y-B and Xu Y 2021 Symmetry-protected topological phases in a Rydberg glass *Phys. Rev. Lett.* **127** 263004

[41] Yi T-C, Hu S, Castro E V and Mondaini R 2021 Interplay of interactions, disorder, and topology in the Haldane–Hubbard model *Phys. Rev.* B **104** 195117

[42] Zhang W, Zou D, Pei Q, He W, Bao J, Sun H and Zhang X 2021 Experimental observation of higher-order topological Anderson insulators *Phys. Rev. Lett.* **126** 146802

[43] Liu G-G *et al* 2020 Topological Anderson insulator in disordered photonic crystals *Phys. Rev. Lett.* **125** 133603

[44] Meier E J, An F A, Dauphin A, Maffei M, Massignan P, Hughes T L and Gadway B 2018 Observation of the topological Anderson insulator in disordered atomic wires *Science* **362** 929

[45] Zangeneh-Nejad F and Fleury R 2020 Disorder-induced signal filtering with topological metamaterials *Adv. Mater.* **32** 2001034

[46] Stützer S, Plotnik Y, Lumer Y, Titum P, Lindner N H, Segev M, Rechtsman M C and Szameit A 2018 Photonic topological Anderson insulators *Nature* **560** 461

[47] Harper P G 1955 Single band motion of conduction electrons in a uniform magnetic field *Proc. Phys. Soc.* A **68** 874

[48] Aubry S and Andre G 1980 Analyticity breaking and Anderson localization in incommensurate lattices *Ann. Israel Phys. Soc.* **3** 133

[49] Li X, Pixley J H, Deng D-L, Ganeshan S and Das Sarma S 2016 Quantum nonergodicity and Fermion localization in a system with a single-particle mobility edge *Phys. Rev.* B **93** 184204

[50] Chang I, Ikezawa K and Kohmoto M 1997 Multifractal properties of the wave functions of the square-lattice tight-binding model with next-nearest-neighbor hopping in a magnetic field *Phys. Rev.* B **55** 12971

[51] Liu F, Ghosh S and Chong Y D 2015 Localization and adiabatic pumping in a generalized Aubry–André–Harper model *Phys. Rev.* B **91** 014108

[52] Wang Y, Cheng C, Liu X-J and Yu D 2021 Many-body critical phase: extended and nonthermal *Phys. Rev. Lett.* **126** 080602

[53] Wang Y, Zhang L, Niu S, Yu D and Liu X-J 2020 Realization and detection of non-ergodic critical phases in an optical Raman lattice *Phys. Rev. Lett.* **125** 073204

[54] Tang L-Z, Zhang G-Q, Zhang L-F and Zhang D-W 2021 Localization and topological transitions in non-Hermitian quasiperiodic lattices *Phys. Rev.* A **103** 033325

[55] Xiao T, Xie D, Dong Z, Chen T, Yi W and Yan B 2021 Observation of topological phase with critical localization in a quasi-periodic lattice *Sci. Bull.* **66** 2175

[56] Botzung T, Vodola D, Naldesi P, Müller M, Ercolessi E and Pupillo G 2019 Algebraic localization from powerlaw couplings in disordered quantum wires *Phys. Rev.* B **100** 155136

[57] Cao X, Rosso A, Bouchaud J-P and Doussal P L 2017 Genuine localization transition in a long-range hopping model *Phys. Rev.* E **95** 062118

[58] Deng X, Ray S, Sinha S, Shlyapnikov G V and Santos L 2019 One-dimensional quasicrystals with powerlaw hopping *Phys. Rev. Lett.* **123** 025301

[59] Deng X, Kravtsov V, Shlyapnikov G and Santos L 2018 Duality in power-law localization in disordered one-dimensional systems *Phys. Rev. Lett.* **120** 110602

[60] Hsu H-C and Chen T-W 2020 Topological Anderson insulating phases in the long-range Su–Schrieffer–Heeger model *Phys. Rev.* B **102** 205425

[61] Pérez-González B, Bello M, Gómez-León Á and Platero G 2019 Interplay between long-range hopping and disorder in topological systems *Phys. Rev.* B **99** 035146

[62] Pérez-González B, Bello M, Gómez-León Á and Platero G 2018 SSH model with long-range hoppings: topology, driving and disorder arXiv:1802.03973 [cond-mat.mes-hall]

[63] Song J and Prodan E 2014 AIII and BDI topological systems at strong disorder *Phys. Rev.* B **89** 224203

[64] Zurek W H 1985 Cosmological experiments in superfluid helium? *Nature* **317** 505

[65] Kibble T 1980 Some implications of a cosmological phase transition *Phys. Rep.* **67** 183

[66] Dziarmaga J 2005 Dynamics of a quantum phase transition: exact solution of the quantum Ising model *Phys. Rev. Lett.* **95** 245701

[67] Damski B 2005 The simplest quantum model supporting the Kibble–Zurek mechanism of topological defect production: Landau–Zener transitions from a new perspective *Phys. Rev. Lett.* **95** 035701

[68] Ruutu V M H, Eltsov V B, Gill A J, Kibble T W B, Krusius M, Makhlin Y G, Plaçais B, Volovik G E and Xu W 1996 Vortex formation in neutronirradiated superfluid ^{3}He as an analogue of cosmological defect formation *Nature* **382** 334

[69] Yukalov V, Novikov A and Bagnato V 2015 Realization of inverse Kibble–Zurek scenario with trapped bose gases *Phys. Lett.* A **379** 1366

[70] Damski B and Zurek W H 2008 How to fix a broken symmetry: quantum dynamics of symmetry restoration in a ferromagnetic Bose–Einstein condensate *New J. Phys.* **10** 045023

[71] Damski B and Zurek W H 2009 Quantum phase transition in space in a ferromagnetic spin-1 Bose–Einstein condensate *New J. Phys.* **11** 063014

[72] Ulm S *et al* 2013 Observation of the Kibble–Zurek scaling law for defect formation in ion crystals *Nat. Commun.* **4** 2290

[73] Pyka K *et al* 2013 Topological defect formation and spontaneous symmetry breaking in ion coulomb crystals *Nat. Commun.* **4** 2291

[74] Cui J-M *et al* 2016 Experimental trapped-ion quantum simulation of the Kibble–Zurek dynamics in momentum space *Sci. Rep.* **6** 33381

[75] Ai M-Z, Cui J-M, He R, Qian Z-H, Gao X-X, Huang Y-F, Li C-F and Guo G-C 2021 Experimental verification of anti-Kibble–Zurek behavior in a quantum system under a noisy control field *Phys. Rev.* A **103** 012608

[76] Gong M *et al* 2016 Simulating the Kibble–Zurek mechanism of the Ising model with a superconducting qubit system *Sci. Rep.* **6** 22667

[77] Gao Z-P, Zhang D-W, Yu Y and Zhu S-L 2017 Anti-Kibble–Zurek behavior of a noisy transverse-field XY chain and its quantum simulation with two-level systems *Phys. Rev.* B **95** 224303

[78] Bermudez A, Patanè D, Amico L and Martin- Delgado M A 2009 Topology-induced anomalous defect production by crossing a quantum critical point *Phys. Rev. Lett.* **102** 135702

[79] Bermudez A, Amico L and Martin-Delgado M A 2010 Dynamical delocalization of Majorana edge states by sweeping across a quantum critical point *New J. Phys.* **12** 055014

[80] Yue S, Zhou X-F and Zhou Z-W 2021 Quench dynamics in 1D model with 3rd-nearest-neighbor hoppings *Chin. Phys.* B **30** 026402

[81] Sacramento P D 2014 Fate of Majorana fermions and Chern numbers after a quantum quench *Phys. Rev.* E **90** 032138

[82] Lee M, Han S and Choi M-S 2015 Kibble–Zurek mechanism in a topological phase transition *Phys. Rev.* B **92** 035117

[83] Fläschner N, Vogel D, Tarnowski M, Rem B S, Lühmann D-S, Heyl M, Budich J C, Mathey L, Sengstock K and Weitenberg C 2017 Observation of dynamical vortices after quenches in a system with topology *Nat. Phys.* **14** 265

[84] Ulčakar L, Mravlje J, Ramšak A and Rejec T 2018 Slow quenches in two-dimensional time-reversal symmetric Z_2 topological insulators *Phys. Rev. B* **97** 195127

[85] Ulˇcakar L, Mravlje J and Rejec T 2019 Slow quenches in Chern insulator ribbons *Phys. Rev.* B **100** 125110

[86] Ulˇcakar L, Mravlje J and Rejec T 2020 Kibble-zurek behaviour in disordered chern insulators *Phys. Rev. Lett.* **125** 216601

[87] Crowley P, Martin I and Chandran A 2020 Half-integer quantized topological response in quasiperiodically driven quantum systems *Phys. Rev. Lett.* **125** 100601

[88] Tong X, Meng Y-M, Jiang X, Lee C, de Moraes Neto G D and Xianlong G 2021 Dynamics of a quantum phase transition in the aubry-andr´e-harper model with p-wave superconductivity *Phys. Rev. B* **103** 104202

[89] Sinha A, Rams M M and Dziarmaga J 2019 Kibble–Zurek mechanism with a single particle: dynamics of the localization-delocalization transition in the Aubry–André model *Phys. Rev.* B **99** 094203

[90] Lu Z, Xu Z and Zhang Y 2022 Mobility edges in topological anderson insulating phase induced by a slowly varying modulation arXiv:2201.00488 [cond-mat.dis-nn]

[91] Tang L-Z, Liu S-N, Zhang G-Q and Zhang D-W 2022 Topological anderson insulators with different bulk states in quasiperiodic chains arXiv:2201.00988 [cond-mat.mes-hall]

[92] Chiu C-K, Teo J C Y, Schnyder A P and Ryu S 2016 Classification of topological quantum matter with symmetries *Rev. Mod. Phys.* **88** 035005

[93] Yao S and Wang Z 2018 Edge states and topological invariants of non-hermitian systems *Phys. Rev. Lett.* **121** 086803

[94] Rufo S, Lopes N, Continentino M A and Griffith M A R 2019 Multicritical behavior in topological phase transitions *Phys. Rev.* B **100** 195432

[95] MacKinnon A and Kramer B 1983 The scaling theory of electrons in disordered solids: additional numerical results *Z. Phys.* B **53** 1

[96] Dziarmaga J 2010 Dynamics of a quantum phase transition and relaxation to a steady state *Adv. Phys.* **59** 1063

[97] Hendry P C, Lawson N S, Lee R A M, McClintock P V E and Williams C D H 1994 Generation of defects in superfluid ^{4}He as an analogue of the formation of cosmic strings *Nature* **368** 315

[98] B. D´ora M, Heyl and Moessner R 2019 The Kibble–Zurek mechanism at exceptional points *Nat. Commun.* **10** 2254

[99] Dziarmaga J 2006 Dynamics of a quantum phase transition in the random ising model: logarithmic dependence of the defect density on the transition rate *Phys. Rev.* B **74** 064416

[100] Zener C 1932 Non-adiabatic crossing of energy levels *Proc. R. Soc.* A **137** 696

[101] Weinmann A 1959 Quantum mechanics (non-relativistic theory.) by L. D. Landau and E. M. Lifshitz. Translated from the Russian by J. B. Sykes and J. S. Bell pp. 515 *Math. Gaz.* **43** 305

[102] Dziarmaga J and Rams M M 2010 Adiabatic dynamics of an inhomogeneous quantum phase transition: the case of a $z > 1$ dynamical exponent *New J. Phys.* **12** 103002